Materials Advances

ROYAL SOCIETY OF CHEMISTRY

PAPER

View Article Online
View Journal | View Issue

Cite this: *Mater. Adv.*, 2024, 5, 4421

A coral-like nano-PCF composite as a broad-bandwidth microwave absorber†

Aiqiong Wang, [a] Jianxiong Li[b] and Xiaoming Zhao*[a]

Received 31st December 2023,
Accepted 10th February 2024

DOI: 10.1039/d3ma01189e

rsc.li/materials-advances

The bandwidth of microwave interference (MWI) has broadened with the increase of portable and intelligent electronics properties due to the diversification of irradiation frequencies. To shield against MWI over a broadened bandwidth, a coral-like polyaniline (PANI)/$CoFe_2O_4$ (CFO) nanocomposite (PCF) microwave absorber (MWA) was synthesized using a sol–gel self-propagation combustion method and annealing process. Computer simulation technology in CST MWS® accurately obtains the optimal thickness for the broadest-bandwidth MWA. The results demonstrated that the minimal reflection loss (RL_{min}) of the coral-like nano-PCF was −61.4 dB at 13.4 GHz with a thickness of 1.96 mm. Further optimization revealed that the effective absorbing bandwidth (EAB) of the coral-like nano-PCF was 6.4 GHz with a thickness of 1.74 mm, and the RL curve obtained from the simulation was in good agreement with the corresponding RL curve obtained experimentally. The strategy provides a new approach for the accurate design of broad-bandwidth MWAs.

1. Introduction

With the advancement of modern wireless communication, in particular the increasing demand for 5G technology, different types of microwave absorbers (MWAs) have been developed to shield against the broadening bandwidth of electromagnetic interference (EMI) in the microwave frequency range 2–18 GHz.[1,2]

A magneto-dielectric synergistic microwave absorber formed by coating polyaniline (PANI) on the surface of $CoFe_2O_4$ (CFO), has demonstrated excellent microwave absorption due to the dielectric loss of PANI synergized with the great magnetic loss of CFO,[3,4] in which PANI and CFO consumed the electric and magnetic components of the microwaves, respectively, and the microwave absorption was enhanced when they were synergized with each other.[5] Praveena *et al.*[6] synthesized a PCF composite to shield against EMI. The results showed that the RL_{min} was −38.7 dB at 17.1 GHz, and the bandwidth of PCF was about 4 GHz around the X band. However, the structure and amorphous nature of PCF enhanced the reflection of incident microwaves, which broadened the bandwidth of microwave absorption *via* the generation of a multi-reflection structure,[7] for example, a coral-like structure,[8] a porous hollow carbon sphere,[9] a core/shell structure,[10] a heterointerface,[11] or nanoparticles.[12] The novel coral-like PCF-5 was found to possess the optimum electromagnetic parameters for enhanced microwave absorption.

To obtain broad-bandwidth MWAs, PCF composites have been synthesised and simulations undertaken using the professional microwave simulation technology CST MWS®.[13] Ning *et al.*[14] prepared a MWA containing multi-walled carbon nanotubes (MWCNTs) and analyzed the microwave absorption using CST MWS®. The results revealed that the effective absorbing bandwidth (EAB) was 12.6 GHz with a thickness of 2.3 mm. Xu *et al.*[15] prepared a carbon aerogel MWA embedded with Co@C nanoparticles and analyzed the microwave absorption using CST MWS®. The RL_{min} was −45.02 dB with a thickness of 1.5 mm, and the EAB was 13.12–17.14 GHz. The experimental results were in good agreement with the simulation results of MWAs.

In this paper, a series of nano-PCFs were produced *via* the citrate gel method combined with ultrasound and stirring[16–18] then the optimal electromagnetic parameters of PCF were selected and the materials tested using CST MWS® to determine their dispersion parameters. Simulation and further optimization of the optimal PCF took place to obtain a MWA that possessed the broadest EAB in the frequency range of interest of 2–18 GHz. Comparing the parameters of the simulation and experiment, we judged that the trends between them were extremely similar. The strategy may provide a new method to obtain a broadest bandwidth MWA in a precise way.

[a] *School of Textile Science and Engineering, Tiangong University, No. 399 Jingwu Xiqing, Tianjin 300387, China. E-mail: texzhao@163.com*
[b] *School of Electronic & Information Engineering, Tiangong University, Tianjin 300387, China*

† Electronic supplementary information (ESI) available. See DOI: https://doi.org/10.1039/d3ma01189e

2. Experiments

2.1 Materials

$Co(NO_3)_2{\cdot}6H_2O$, $Fe(NO_3)_3{\cdot}9H_2O$, NaOH, citric acid, ammonium persulfate (Alfa Aesar), hydrochloric acid (Aladdin), and anhydrous ethanol (Macklin) were obtained.

2.2 The synthesis of nano-$CoFe_2O_4$ using a sol–gel self-propagating combustion method and annealing[19,20]

Uniform nanoscale cobalt ferrite $CoFe_2O_4$ was prepared using a facile sol–gel self-propagating combustion method. $Co(NO_3)_2{\cdot}6H_2O$, $Fe(NO_3)_3{\cdot}9H_2O$, and citric acid were weighed according to their stoichiometric ratio ($M_{Co^{2+}}:M_{Fe^{3+}}:M_{citric\ acid}$ = 1 : 2 : 1.2) and dissolved in 50 mL anhydrous ethanol. The mixture was magnetically stirred at room temperature for 1 h to obtain a homogeneous solution. The precursors were adjusted to a pH of 9 by the dropwise addition of saturated NaOH solution. The mixture was transferred into a 200 mL crucible and then combusted. After extinguishing, a gel was observed to have formed, and the gel was annealed in a Muffle furnace under atmospheric conditions. The temperature was raised from room temperature to 750 °C at a rate of 5 °C min^{-1}. After holding at the temperature of 750 °C for 1 h, the hybrid cooled slowly naturally. The nanoparticle cobalt ferrite $CoFe_2O_4$ (CFO) was formed. The chemical equations are shown below:

$$Co(NO_3)_2{\cdot}6H_2O + Fe(NO_3)_3{\cdot}9H_2O + 5OH^- \rightarrow Co(OH)_2 + Fe(OH)_3 + 5NO_3^- + 15H_2O$$

$$Co(OH)_2 + 2Fe(OH)_3 \xrightarrow{750^\circ C} CoFe_2O_4 + 4H_2O$$

2.3 The synthesis of PANI/$CoFe_2O_4$ (PCF) composites[21,22]

After the monomer aniline was injected into a 450 mL beaker containing 150 mL hydrochloric acid solution (containing 25 mL HCl), a certain weight ratio of nano-$CoFe_2O_4$ (CFO) was added. The weight ratios of CFO were 30%, 40%, 50%, and 60%. Ammonium persulfate (APS) hydrochloric acid (27.38 g APS dissolved in 1.8 M hydrochloric acid) was added to the mixture dropwise.[22] The polymerization was carried out at a temperature less than 10 °C *via* a combination of continuous stirring at 400–500 rpm and ultrasonication for 8 h. The reaction mixture was concentrated, filtered, and washed with deionized water and anhydrous ethanol repeatedly until the filtrate was colorless. They were dried in the vacuum oven at 60 °C for 24 h. They were assigned as PCF-3, PCF-4, PCF-5, and PCF-6 because of the weight ratios of the CFO respectively. The illustration of the synthetic process of the PANI/$CoFe_2O_4$ composite is shown in Fig. 1.

2.4 Characteristics

Fourier transform infrared spectroscopy (FTIR, Nicolet iS50) was used to characterize the surface functional groups and chemical bonds of the samples. X-ray diffraction (XRD, D8 ADVANCE(BRUKER)) analysis determined the crystal structure of the samples. Transmission electron microscopy (TEM, Hitachi H7650) patterns and scanning electron microscopy (SEM, FlexSEM1000) images determined the morphology and nanostructure of the material. An automated gas sorption analyzer (Autosorb-iQ, USA) was used to test the porosity. A vector network analyzer (VNA, Agilent E5071C, USA) determined the electromagnetic properties for a sample with a weight ratio of 4 : 6 for nano-PCF to paraffin wax.

3. Selecting the PCF composite with the optimum microwave absorption ability

An excellent absorber should possess a good impedance match and robust reflection loss simultaneously.[23,24] A good impedance matching ability of an absorber means most radiating microwaves penetrate the MWA.[25,26] Significant reflection loss will attenuate the incident microwaves, and the absorption strength may be extended.[27,28]

We inspected the impedance match and reflection loss of PCF-3, PCF-4, PCF-5, and PCF-6 *via* the electromagnetic

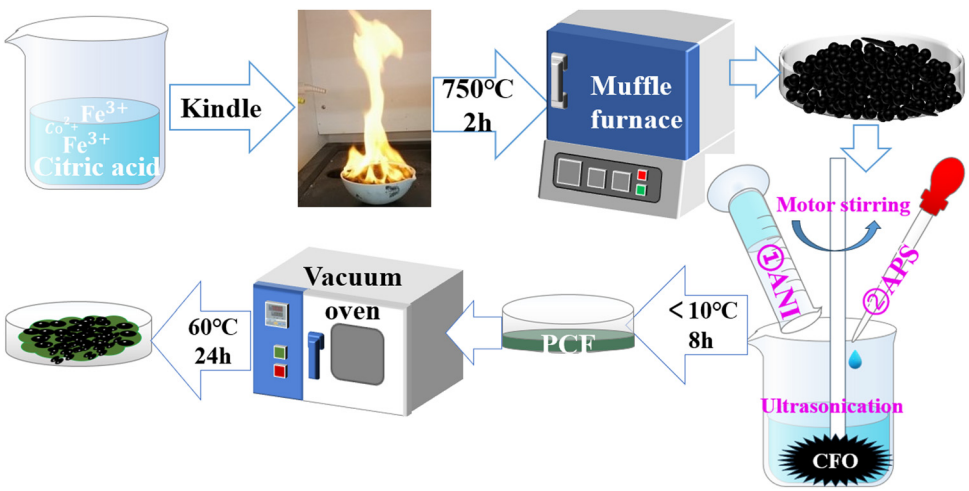

Fig. 1 The illustration of the synthetic process of PCF composites.

parameters tested by the coaxial transmission line method.[29] Eqn (1)–(3) below express the coaxial transmission line theory:[30]

$$Z_{in} = Z_0\sqrt{\frac{\mu_r}{\varepsilon_r}}\tanh\left[j\left(\frac{2\pi fd}{c}\sqrt{\varepsilon_r\mu_r}\right)\right], \quad (1)$$

$$RL = 20\log\left|\frac{Z_{in}-1}{Z_{in}+1}\right|, \quad (2)$$

$$Z_0 = \sqrt{\frac{\mu_0}{\varepsilon_0}}, \quad (3)$$

where ε_r, μ_r, ε_0, and μ_0 refer to the relative complex permittivity and permeability of sample and space, respectively. Z_{in} designates the input impedance of the sample, and Z_0 represents the impedance of free space. f, c, and d refer to the frequency, speed of light, and thickness of the sample.

The reflection loss (RL) value is a significant index of a MWA.[31] We calculated the RL values based on eqn (1) and (2). 2D color contour plots and 3D color maps that exhibit the relationships of the RL to thickness and frequency in the frequency range of 2–18 GHz for the PCF samples were produced and are shown in Fig. 2a–h.

Among the curves, the RL of PCF-5 was optimal. The RL_{min} of PCF-5 was −61.4 dB at 13.4 GHz with a thickness of 1.96 mm, and the EAB was 4.3 GHz in the corresponding condition. The RL_{min} of PCF-3, PCF-4, and PCF-6 were −4.18 dB, −11.7 dB, and −11.45 dB and the EABs of PCF-3, PCF-4, and PCF-6 were 0, 1.5, and 1.53 GHz, respectively. Obviously, the EAB of PCF-5 was the broadest compared to those of the other PCFs. This indicated that the RL of PCF-5 was optimal among the series of PCFs.

In summary, the RL of PCF-5 was the best among the PCFs, which is conducive to the smooth transmission of microwaves through PCF-5 and indicated that the absorption was greatly enhanced. Therefore, simulations and further optimization on PCF-5 were performed using CST MWS® to determine the optimal thickness for the broadest bandwidth.

4. CST simulation

For simulations using CST MWS®, the nano-PCF-5 was modelled as a cuboid with a dimensions of 10 mm × 10 mm × d mm, as shown in Fig. 4g. The nano-PCF-5 was assumed to be distributed evenly in the cuboid. The boundaries were set as the unit cell in the X and Y directions and open in the Z direction. The excitation source was a plane wave. The sweep frequency range was 2–18 GHz.

The results of the simulation experiment were highly in accordance with each other, as shown in Fig. 4h. They revealed that the model and the initial set of parameters for PCF-5 in CST MWS® were suitable, and can be used as the basis for further optimization of PCF-5. The results demonstrated that the broadest EAB of PCF-5 was 6.4 GHz with a thickness of 1.74 mm. The RL curves of the experiment and simulation were in good agreement with each other, as shown in Fig. 4h.

5. Results and discussion

5.1 FTIR

The FTIR spectra of CFO, PANI and PCF-5 confirm the chemical groups present in them, as shown in Fig. 3a. In the figure, the similarity of the results for PCF-5 and PANI was remarkable, with the exception of three peaks. The three FTIR peaks of PCF-5 were hypochromatically shifted and the transmittance promoted entirely compared to PANI, as the peaks at around 1233, 1371, and 503 cm^{-1} in PANI had shifted to 1238, 1358, and 469 cm^{-1}, respectively. This was due to the successful coating of PANI on the surface of the nano-CFO and the generation of a dangling π–π bond interacting between them.[22,32]

The characteristic peaks of PCF-5 were presented as follows: there was a peak around 592 cm^{-1}, which was designated as a typical stretching vibration of the Fe–O bond and characterized the tetrahedral and octahedral sites of the spinel structure of $CoFe_2O_4$.[20,33] The peaks around 499 and 562 cm^{-1} indicated

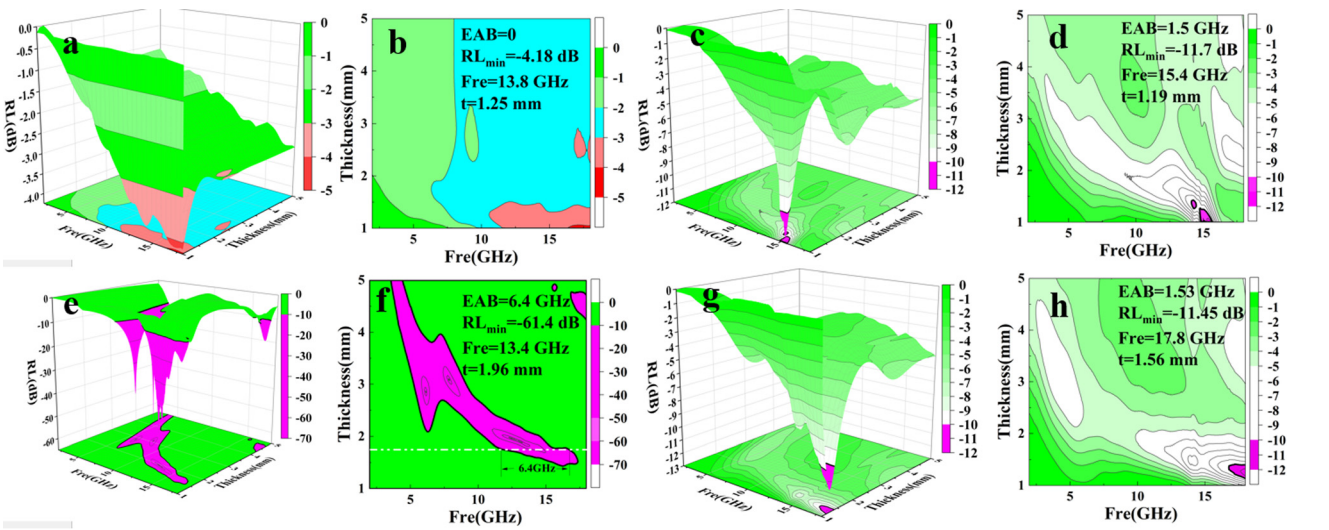

Fig. 2 The reflection loss of the PCF samples with thickness and frequency. (a), (c), (e) and (g) and (b), (d), (f) and (h) are the 3D and 2D color reflection loss contour maps of thickness and frequency of PCF-3, PCF-4, PCF-5, and PCF-6, respectively.

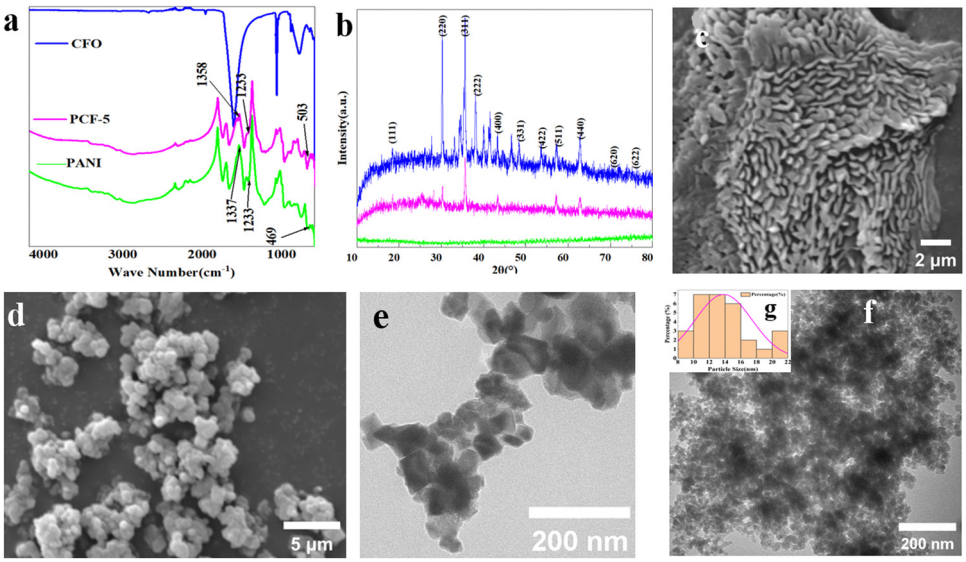

Fig. 3 (a) FTIR spectra of CFO, PANI, and PCF-5. (b) XRD spectra of PCF, CFO and PANI. (c) and (d) SEM images of PCF-5 and CFO, respectively. (e) and (f) TEM patterns of CFO and PCF-5, respectively. (g) Particle size analysis of PCF-5 corresponding to (f).

the vibrations of the Fe–O bond in the composite. The peaks at 1563 and 1481 cm^{-1} represented the vibration of the C=C bond in the quinoid and benzenoid rings. The peak at 1291 cm^{-1} indicated the vibration of a secondary aromatic amine. The peak at 1481 cm^{-1} referred to the vibration of C≡N. The peaks at 780 and 1025 cm^{-1} were assigned to the out-of-plane deformations of C–H. The peak at 3218 cm^{-1} denoted the stretching of an aromatic amine.[34,35]

In summary, the analysis above indicated that the nano-CFO and PANI combined together due to the existence of a π–π bond to form PANI/CFO(PCF).

5.2 XRD

The XRD spectrum of PCF-5 is presented in Fig. 3b, and this displays the same primary diffraction peaks at 2θ = 18.5°, 30°, 36°, 44°, 57°, and 64°, which correspond to the (111), (220), (311), (400), (511), and (440) lattice planes of $CoFe_2O_4$. The crystal planes of PCF-5 located at 38°, 49°, 53.8°, 71.5°, and 75.8° can be indexed to the (222), (331), (422), (620), and (622) crystal planes of PANI based on the JCPDS NO. 29-0513 card and some of the diffraction peaks were shifted slightly. This indicated that the PANI/$CoFe_2O_4$ hybrids were successfully synthesized.

5.3 SEM & TEM

The surface morphologies of nano-$CoFe_2O_4$ and the PCF-5 composite were examined *via* scanning electron microscopy (SEM), and the results are shown in Fig. 3c and d. In Fig. 3d, the CFO nanoparticle was sphere-like, which can be demonstrated by TEM (Fig. 3e and f), and the agglomeration phenomenon of CFO was due to its inherent magnetic performance. The morphology of PCF-5 was coral-like, as shown in Fig. 3c. The coral-like PCF-5 was conducive to the multi-reflection of microwaves, which favored the promoting absorption of PCF-5.[36,37]

TEM images were used to probe the nanostructure of CFO and PCF-5, which was conducive to analyzing the absorption properties of PCF-5, and the results are shown in Fig. 3e and f. In Fig. 3f, it appeared that some dark gray particles (inorganic particles) were wrapped by light gray materials (organic materials),[38,39] which indicated that the inner layer of sphere-like CFO was wrapped by an outer layer of PANI.

Based on the above observations, we inferred that the sphere-like CFO was wrapped with PANI because of the generation of π–π bonds and gradually developed into the coral-like PCF-5. Furthermore, the particles of coral-like PCF-5 had a diameter of 14 ± 4 nm, as shown in Fig. 3f. The particle size analysis of PCF-5 is shown in Fig. 3g.

5.4 Impedance match of PCF-5

The impedance match of PCF-5 indicated that the impedance of PCF-5 matched well with the impedance of free space, as shown in Fig. 4a. The ENIR (effective normalized impedance range) was 8.67 GHz (9.34–18 GHz) with a thickness of 1.8 mm. The excellent impedance match of nano-PCF-5 is mainly due to two features: first, the approximation of moderate dielectric loss tan δ_ε and higher magnetic loss tan $\delta\mu_r$ of PCF-5, as shown in Fig. 4b. To obtain a perfect impedance match, the impedance of the incident material should be as close to that of free space as possible,[40] which indicates that the value of Z_{in}/Z_0 should be as close to 1 as possible. Using eqn (1)–(3), the value $Z_{in}/Z_0 \approx \mu_r/\varepsilon_r$, which meant that the values of μ_r and ε_r should be as close as possible. The theory of impedance matching is consistent with the actual data for PCF-5, which indicated that the approximate magneto-dielectric loss of PCF-5 is related to its excellent impedance match.[40,41]

The second feature contributing to the excellent impedance match of nano-PCF-5 is the mesoporous structure of PCF-5. The N_2 absorption–desorption isotherm is type IV indicating that

PCF-5 is a mesoporous material,[42] as shown in Fig. 4c. The average pore size was 3.4 nm, and the specific surface area was 16.424 $cm^2\ g^{-1}$ with the Brunauer–Emmett–Teller (BET) model.[43] The atmosphere of the interstitial spaces reinforces the compatibility of PCF-5 and free space, and its large specific surface area energy enhances the microwave absorption ability of the mesoporous structure.[44] The mesoporous structure permitted microwave transmission within PCF-5.[45] Furthermore, the multi-scattering and reflection of the mesoporous structure reduced the reflection of microwaves back to space.[46]

5.5 The reflection loss and mechanism of PCF-5

The RL_{min} of PCF-5 is a significant parameter related to its absorption.[47] The RL_{min} is related to the inherent characteristics of PCF-5[48] and the $1/4\lambda$ principle,[49] which stem from the electron hopping and interference polarization, respectively.[50] The RL is related to frequency and thickness, as shown in the 3D color contour and surface plot in Fig. 4d. The RL_{min} of PCF-5 was −61.4 dB at 13.4 GHz with a thickness of 1.96 mm.

There are some clarifications below that reveal the microwave-absorbing mechanism of PCF-5: (1) the moderate relative complex permittivity ($\varepsilon_r = \varepsilon' - j\varepsilon''$) and higher permeability ($\mu_r = \mu' - j\mu''$) of PCF-5,[51] as shown in Fig. 4b. The PANI conducted the electrical components of the microwaves that became polarized, with the degree of polarization denoted as ε_r.[52] The real and imaginary parts of the permittivity were 7–12 and 0–4, respectively, which indicated that the dielectric loss of PCF-5 was moderate.[53] A moderate ε_r was conducive to the absorption characteristics of PCF-5,[54] as it avoided the impedance mismatch and secondary microwave pollution for free space brought on by an excessive ε_r.[55] The nano-$CoFe_2O_4$, a higher magnetic loss MWA, consumed the magnetic components of the microwaves, which both conducted the magnetic energy and complemented the decreasing ε_r of PCF-5.[56] The dielectric loss and magnetic loss had a synergistic effect[57] when PANI was coated on the surface of $CoFe_2O_4$, which enhanced the microwave absorption ability of PCF-5.

(2) The polarization effect of PCF-5. Cole–Cole semicircles of ε'' *versus* ε'[58] for PCF-5 are shown in Fig. 4e. Each Cole–Cole semicircle represents the Debye relaxation behavior derived from eqn (4)–(6).[59] The larger the Cole–Cole semicircle, the stronger the Debye relaxation, which helps to enhance the electromagnetic loss.[60] The line in the Cole–Cole curve represents the conduction loss of PCF-5.[61] The dipole and interface polarity stem from asymmetric distribution of charges at the defect, the heterogeneous surfaces, and the functional groups of PANI and $CoFe_2O_4$.[22]

$$\varepsilon' = \varepsilon_\infty + \frac{\varepsilon_S - \varepsilon_\infty}{1 + (2\pi f)^2\tau^2}, \quad (4)$$

$$\varepsilon'' = \frac{2\pi f\tau(\varepsilon_S - \varepsilon_\infty)}{1 + (2\pi f)^2\tau^2}, \quad (5)$$

$$\left(\varepsilon' - \frac{\varepsilon_S + \varepsilon_\infty}{2}\right) + (\varepsilon'')^2 = \left(\frac{\varepsilon_S - \varepsilon_\infty}{2}\right)^2, \quad (6)$$

where τ, ε_s, and ε_∞ denote the polarization relaxation time, the static permittivity, and the high-frequency limited permittivity, respectively.

(3) The magnetic resonance C_0. C_0 can be expressed as shown in eqn (7). It has been determined that C_0 would be constant if the magnetic loss mainly arose from the eddy current loss.[62] However, the C_0 value of PCF-5 wasn't constant with the increasing of frequency, as shown in Fig. 4f. There was a significant fluctuation in the frequency range of 5–8 GHz, which indicated a strong natural resonance at the corresponding frequency.[63] Slight instability of C_0 occurred in the frequency range of 12–18 GHz, which indicated a relatively mild exchange resonance at the corresponding frequency.[64]

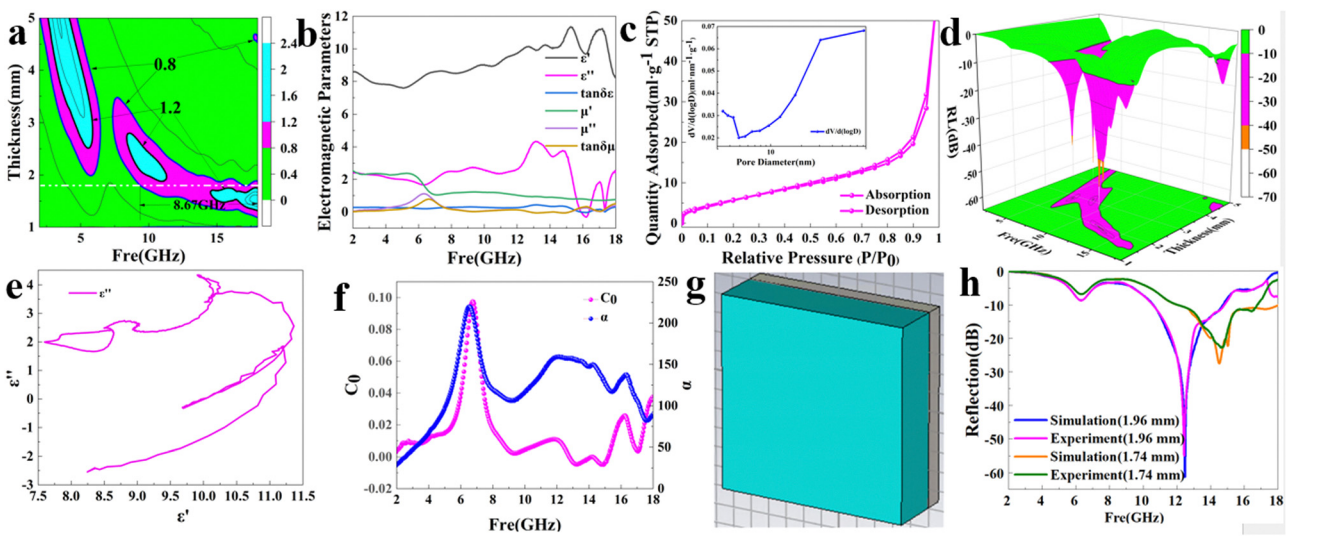

Fig. 4 The absorption of PCF-5. (a) The 3D color contour impedance match. (b) The electromagnetic parameter. (c) The N_2 absorption–desorption isotherm. (d) The 3D color contour and surface diagram. (e) The Cole–Cole semicircle. (f) The C_0 curve and attenuation constants α. (g) The model used in CST MWS®. (h) The comparison of RLs.

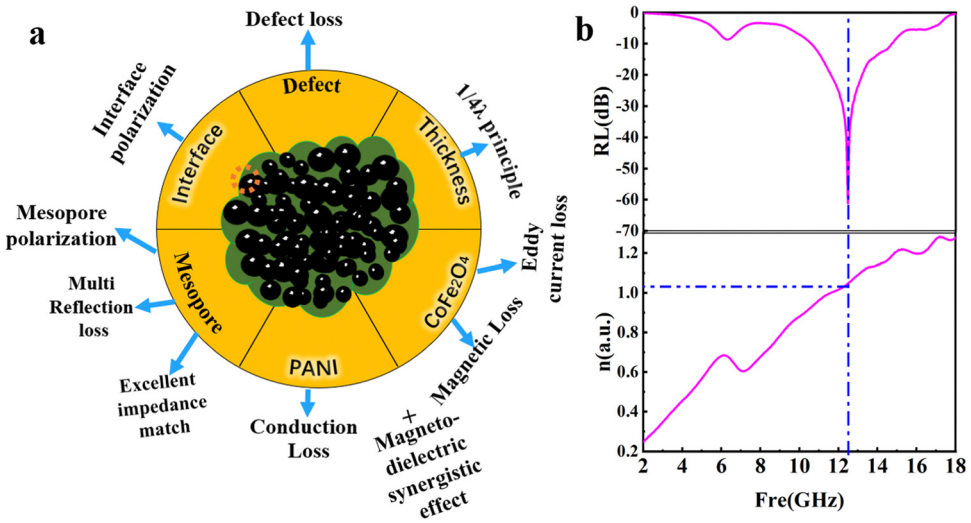

Fig. 5 (a) Illustration of the various microwave-absorption mechanisms of PCF-5. (b) The quarter wavelength (1/4λ) principle of PCF-5.

Furthermore, the fluctuation of C_0 was relatively small in the frequency ranges of 2–5 GHz and 8–12 GHz, and the fluctuation represented the eddy current loss in the corresponding frequency ranges.[65]

$$C_0 = 2\pi\mu_0\sigma d^2/3 = \mu''(\mu')^{-2}f^{-1}, \quad (7)$$

where σ represents the electrical conductivity of an MWA. C_0 refers to the magnetic resonance of PCF-5.

(4) The mesoporous structure of PCF-5. The mesoporous structure prolonged the microwave propagation pathway, which enhanced the dissipation ability of PCF-5.[66] The specific surface energy of the mesoporous structure reinforced the wave-absorbing ability of PCF-5.[44]

(5) The quarter-wavelength (1/4λ) principle. The model shows that when the thickness of an MWA satisfies eqn (8) and the frequency changes, comprehensive interference occurs between the upper and the lower surfaces, which eliminates the reflection loss of the MWA and enhances its microwave-absorbing ability.[67] When the thickness of PCF-5 was 1.96 mm, the thickness almost satisfied eqn (8) at the frequency 13.4 GHz, as shown in Fig. 5b, which indicated that there was comprehensive interference between the upper and lower surfaces of PCF-5, and the microwave absorption of PCF-5 was enhanced.

$$d_m = \frac{nc}{4f_m\sqrt{|\mu_r||\varepsilon_r|}} \quad (n = 1,\ 3,\ 5, \ldots), \quad (8)$$

where μ_r and ε_r represent the complex relative permeability and permittivity of PCF-5 at f_m, and d_m and f_m are the thickness and frequency of the most enhanced PCF-5, respectively.

Generally, the microwave-absorption ability of PCF-5 depended on the electromagnetic parameters, polarization effect, magnetic resonance, mesoporous structure and the quarter wavelength (1/4λ) principle. The attenuation constant α represented the complex damping ability of PCF-5, which is a measure of the microwave absorption, as calculated using eqn (9).[68] The correlation between the attenuation constant α and frequency is shown in Fig. 4f. The fluctuation trend of α is similar to that of C_0 of PCF-5, indicating that the robust magnetic loss of CFO played an important role in the absorption properties of PCF-5.[69]

$$\alpha = \frac{\sqrt{2}\pi f}{c} \times \sqrt{(\mu''\varepsilon'' - \mu'\varepsilon') + \sqrt{(\mu'\varepsilon'' + \mu''\varepsilon')^2 + (\mu''\varepsilon'' - \mu\varepsilon'')^2}} \quad (9)$$

In summary, the coral-like nano-PCF-5 is endowed with the synergistic effects of moderate permittivity and higher permeability, defects, interfaces and mesoporous structure to provide a robust attenuation ability for the absorption of microwaves, as shown in Fig. 5.

6. Conclusions

In conclusion, the coral-like cobalt ferrite $CoFe_2O_4$ nanomaterial was prepared by a sol–gel self-propagating combustion method. The nano-PCF composite was synthesized *via* coating the surface of CFO with PANI to develop the coral-like structure. A series of comparisons were made on the electromagnetic parameters of the PCF samples, and the optimal PCF was selected for simulation, and a broad-bandwidth PCF was accurately prepared. The results revealed that the microwave absorption of PCF-5 was optimum, and the RL_{min} of PCF-5 was −61.4 dB at 13.4 GHz with a thickness of 1.96 mm. Further optimization using CST MWS® demonstrated that the broadest EAB of PCF-5 was 6.2 GHz with a thickness of 1.74 mm. The results of experiment and simulation were in good agreement. The strategy provides a new approach for the accurate design of broad-bandwidth MWAs.

Conflicts of interest

The authors declare no competing financial interests.

References

1 Z. L. Du, D. S. Wang, X. F. Zhang and Z. Y. Yi, *et al.*, Core–Shell Structured SiO_2@NiFe LDH Composite for Broadband Electromagnetic Wave Absorption, *Int. J. Mol. Sci.*, 2023, **24**(1), 504, DOI: 10.3390/ijms24010504.

2 A. Q. Wang, J. X. Li, C. Meng and X. M. Zhao, A review of graphene-based broad bandwidth microwave absorbing textile-based composites in the low-frequency range, *J. Ind. Text.*, 2022, **52**, DOI: 10.1177/15280837221133113.

3 H. Luo, B. B. Ma, F. Chen and S. S. Zhang, *et al.*, Bimetallic Oxalate Rod-Derived NiFe/Fe_3O_4@C Composites with Tunable Magneto-dielectric Properties for High-Performance Microwave Absorption, *J. Phys. Chem. C*, 2021, **125**(44), 24540–24549, DOI: 10.1021/acs.jpcc.1c04386.

4 P. F. Huang, Y. W. Wang, M. A. El-Shorbagy and M. N. Akhtar, *et al.*, Optical and electromagnetic absorption features of hierarchical pampon and cauliflower-like magneto/dielectric composite based absorber for C and X bands application, *Ceram. Int.*, 2022, **48**(11), 16280–16289, DOI: 10.1016/j.ceramint.2022.02.177.

5 Y. Akinay, U. Gunes, B. Çolak and T. Cetin, Recent progress of electromagnetic wave absorbers: a systematic review and bibliometric approach, *Chem. Phys. Mater.*, 2023, **2**(3), 197–206.

6 K. Praveena and M. Bououdina, Tunable Microwave Absorbing Properties of $CoFe_2O_4$/PANI Nanocomposites, *J. Electron. Mater.*, 2020, **49**(10), 6187–6198, DOI: 10.1007/s11664-020-08352-y.

7 H. Zhang, J. Cheng, H. Wang and Z. Huang, *et al.*, Initiating VB-Group Laminated NbS_2 Electromagnetic Wave Absorber toward Superior Absorption Bandwidth as Large as 6.48 GHz through Phase Engineering Modulation, *Adv. Funct. Mater.*, 2022, **32**(6), 2108194.

8 T. H. Ting, Y. N. Jau and R. P. Yu, Microwave absorbing properties of polyaniline/multi-walled carbon nanotube composites with various polyaniline contents, *Appl. Surf. Sci.*, 2012, **258**(7), 3184–3190, DOI: 10.1016/j.apsusc.2011.11.061.

9 X. Guan, Z. Yang, Y. Zhu and L. Yang, *et al.*, The controllable porous structure and s-doping of hollow carbon sphere synergistically act on the microwave attenuation, *Carbon*, 2022, **188**, 1–11.

10 Z. Wu, H.-W. Cheng, C. Jin and B. Yang, *et al.*, Dimensional Design and Core–Shell Engineering of Nanomaterials for Electromagnetic Wave Absorption, *Adv. Mater.*, 2022, **34**(11), 2107538.

11 L. Liang, W. Gu, Y. Wu, B. Zhang, G. Wang, Y. Yang and G. Ji, Heterointerface Engineering in Electromagnetic Absorbers: New Insights and Opportunities, *Adv. Mater.*, 2022, **34**(4), 2106195.

12 R. Peymanfar and S. Javanshir, Preparation and characterization of $Ba_{0.2}Sr_{0.2}La_{0.6}MnO_3$ nanoparticles and investigation of size & shape effect on microwave absorption, *J. Magn. Magn. Mater.*, 2017, **432**, 444–449.

13 Z. X. Xu, L. D. Kong, W. G. Lin and B. F. Jia, Microwave characteristic simulation research for a kind of novel electromagnetic structure, *J. Syst. Eng. Electron.*, 2008, **19**(3), 467–472.

14 M. Q. Ning, P. H. Jiang, W. Ding and X. B. Zhu, *et al.*, Phase Manipulating toward Molybdenum Disulfide for Optimizing Electromagnetic Wave Absorbing in Gigahertz, *Adv. Funct. Mater.*, 2021, **31**(19), 2011229, DOI: 10.1002/adfm.202011229.

15 B. G. Xu, D. G. Zhang, Y. Wang and B. B. Hong, *et al.*, Characterization of millimeter wave photonic crystal circulator with a ferrite sphere, *Results Phys.*, 2022, **34**, 105315, DOI: 10.1016/j.rinp.2022.105315.

16 R. Peymanfar and N. Khodamoradipoor, Preparation and Characterization of Copper Chromium Oxide Nanoparticles Using Modified Sol-Gel Route and Evaluation of Their Microwave Absorption Properties, *Phys. Status Solidi A*, 2019, **216**(11), 1900057, DOI: 10.1002/pssa.201900057.

17 R. Peymanfar, E. Selseleh-Zakerin, A. Ahmadi and A. Sharifi, *et al.*, Regulating microwave absorption and energy bandgap using cauliflower-like polyaniline coated on $La_{0.8}Sr_{0.2}FeO_3$ nanoparticles, *J. Mater. Sci.: Mater. Electron.*, 2021, **32**(21), 25679–25687, DOI: 10.1007/s10854-020-04203-y.

18 R. Peymanfar, F. Norouzi and S. Javanshir, Preparation and characterization of one-pot PANi/Fe/Fe_3O_4/Fe_2O_3 nanocomposite and investigation of its microwave, magnetic and optical performance, *Synth. Met.*, 2019, **252**, 40–49, DOI: 10.1016/j.synthmet.2019.04.008.

19 B. Shi, H. S. Liang, Z. J. Xie and Q. Chang, *et al.*, Dielectric loss enhancement induced by the microstructure of $CoFe_2O_4$ foam to realize broadband electromagnetic wave absorption, *Int. J. Miner., Metall. Mater.*, 2023, **30**(7), 1388–1397, DOI: 10.1007/s12613-023-2599-4.

20 N. Kasapoglu, A. Baykal, Y. Koseoglu and M. S. Toprak, Microwave-assisted combustion synthesis of $CoFe_2O_4$ with urea, and its magnetic characterization, *Scr. Mater.*, 2007, **57**(5), 441–444, DOI: 10.1016/j.scriptamat.2007.04.042.

21 H. B. Yang, N. Han, Y. Lin and G. Zhang, *et al.*, Enhanced microwave absorbing properties of PANI/$CoFe_2O_4$/PVDF composite, *RSC Adv.*, 2016, **6**(102), 100585–100589, DOI: 10.1039/c6ra19885f.

22 E. E. Tanriverdi, A. T. Uzumcu, H. Kavas and A. Demir, *et al.*, Conductivity Study of Polyaniline–Cobalt Ferrite (PANI-$CoFe_2O_4$) Nanocomposite, *Nano-Micro Lett.*, 2011, **3**(2), 99–107, DOI: 10.1007/BF03353658.

23 W. Zheng, W. X. Ye, P. Yang and D. S. Wang, *et al.*, Recent Progress in Iron-Based Microwave Absorbing Composites: A Review and Prospective, *Molecules*, 2022, **27**(13), 4117, DOI: 10.3390/molecules27134117.

24 F. B. Meng, H. G. Wang, F. Huang and Y. F. Guo, *et al.*, Graphene-based microwave absorbing composites: a review and prospective, *Composites, Part B*, 2018, **137**, 260–277, DOI: 10.1016/j.compositesb.2017.11.023.

25 L. Wang, Q. C. Quan, L. L. Zhang and L. C. Cheng, *et al.*, Microwave absorption of NdFe magnetic powders tuned with impedance matching, *J. Magn. Magn. Mater.*, 2018, **449**, 385–389, DOI: 10.1016/j.jmmm.2017.10.067.

26 Y. Huang, J. D. Ji, Y. Chen and X. Li, *et al.*, Broadband microwave absorption of Fe_3O_4–$BaTiO_3$ composites

enhanced by interfacial polarization and impedance matching, *Composites, Part B*, 2019, **163**, 598–605, DOI: 10.1016/j.compositesb.2019.01.008.

27 Y. Liu, K. Zhao, M. G. B. Drew and Y. Liu, A theoretical and practical clarification on the calculation of reflection loss for microwave absorbing materials, *AIP Adv.*, 2018, **8**(1), 015223, DOI: 10.1063/1.4991448.

28 N. H. Faisal, R. Ahmed, N. Sellami and A. Prathuru, *et al.*, Thermal Spray Coatings for Electromagnetic Wave Absorption and Interference Shielding: A Review and Future Challenges, *Adv. Eng. Mater.*, 2022, **24**(7), 2200171, DOI: 10.1002/adem.202200171.

29 R. Peymanfar and A. Mirkhan, Biomass-derived materials: promising, affordable, capable, simple, and lightweight microwave absorbing structures, *Chem. Eng. J.*, 2022, **446**, 136903, DOI: 10.1016/j.cej.2022.136903.

30 J. Xu, Y. H. Cui, J. Q. Wang and Y. H. Fan, *et al.*, Fabrication of wrinkled carbon microspheres and the effect of surface roughness on the microwave absorbing properties, *Chem. Eng. J.*, 2020, **401**, 126027, DOI: 10.1016/j.cej.2020.126027.

31 R. B. Yang, P. M. Reddy, C. J. Chang and P. A. Chen, *et al.*, Synthesis and characterization of Fe_3O_4/polypyrrole/carbon nanotube composites with tunable microwave absorption properties: role of carbon nanotube and polypyrrole content, *Chem. Eng. J.*, 2016, **285**, 497–507, DOI: 10.1016/j.cej.2015.10.031.

32 H. J. Deng, Q. Li, J. J. Liu and F. Wang, Active sites for oxygen reduction reaction on nitrogen-doped carbon nanotubes derived from polyaniline, *Carbon*, 2017, **112**, 219–229, DOI: 10.1016/j.carbon.2016.11.014.

33 A. Baykal, N. Kasapoğlu, Y. Köseoğlu and A. Başaran, *et al.*, Microwave-induced combustion synthesis and characterization of $Ni_xCo_{1-x}Fe_2O_4$ nanocrystals (x = 0.0, 0.4, 0.6, 0.8, 1.0), *Open Chem.*, 2008, **6**(1), 125–130, DOI: 10.2478/s11532-007-0070-4.

34 Z. Durmus, A. Baykal, H. Kavas and H. Sozeri, Preparation and characterization of polyaniline (PANI)-Mn_3O_4 nanocomposite, *Phys. B: Condens. Matter*, 2011, **406**(5), 1114–1120, DOI: 10.1016/j.physb.2010.12.059.

35 V. Gautam, A. Srivastava, K. P. Singh and V. L. Yadav, Vibrational and gravimetric analysis of polyaniline/polysaccharide composite materials, *Polym. Sci., Ser. A*, 2016, **58**(2), 206–219, DOI: 10.1134/s0965545x16020085.

36 M. Green, Y. Li, Z. H. Peng and X. B. Chen, Dielectric, magnetic, and microwave absorption properties of polyoxometalate-based materials, *J. Magn. Magn. Mater.*, 2020, **497**, 165974, DOI: 10.1016/j.jmmm.2019.165974.

37 E. J. Murphy, B. S. Hensley, S. T. Linden and B. T. Draine, *et al.*, Where's the Dust? The Deepening Anomaly of Microwave Emission in NGC 4725 B, *Astrophys. J. Lett.*, 2020, **905**(2), L23, DOI: 10.3847/2041-8213/abc7c8.

38 Z. F. Zhang, J. H. Liang, J. L. Wang and Y. T. Zheng, *et al.*, Resolving Mixed Intermediate Phases in Methylammonium-Free Sn–Pb Alloyed Perovskites for High-Performance Solar Cells, *Nano-Micro Lett.*, 2022, **14**(1), 165, DOI: 10.1007/s40820-022-00918-1.

39 M. T. Nguyen, K. Yu, T. Tokunaga and K. Boonyaperm, *et al.*, Green Synthesis of Size-Tunable Iron Oxides and Iron Nanoparticles in a Salt Matrix, *ACS Sustainable Chem. Eng.*, 2019, **7**(21), 17697–17705, DOI: 10.1021/acssuschemeng.9b03950.

40 X. L. Liu, J. M. Xue, F. Yang and F. Ye, *et al.*, Design and fabrication of Al_2O_3f/SiCN composite with excellent microwave absorbing and mechanical properties, *J. Am. Ceram. Soc.*, 2020, **103**(11), 6255–6264, DOI: 10.1111/jace.17326.

41 H. Y. Zhang, F. Cao, H. Xu and W. Tian, *et al.*, Plasma-enhanced interfacial engineering of FeSiAl@PUA@SiO_2 hybrid for efficient microwave absorption and anti-corrosion, *Nano Res.*, 2023, **16**(1), 645–653, DOI: 10.1007/s12274-022-5100-1.

42 W. H. Huang, S. Wang, X. F. Yang and X. X. Zhang, *et al.*, Temperature induced transformation of Co@C nanoparticle in 3D hierarchical core–shell nanofiber network for enhanced electromagnetic wave adsorption, *Carbon*, 2022, **195**, 44–56, DOI: 10.1016/j.carbon.2022.04.019.

43 Y. Zhang, Y. Sun, Q. B. Che and X. Q. Li, Hydroxymethyl-Functionalized Polymer Nanospheres with a Hollow Mesopore Structure for Efficient Acteoside Adsorption, *ACS Appl. Nano Mater.*, 2023, **6**(17), 15841–15850, DOI: 10.1021/acsanm.3c02751.

44 Z. H. Zhang, G. Y. Zhang, L. M. Lei and H. D. Yuan, *et al.*, One-step synthesis of Fe nanoparticles wrapped in N-doped carbon nanohorn microspheres as high-performance electromagnetic wave absorber, *Ceram. Int.*, 2022, **48**(13), 18338–18347, DOI: 10.1016/j.ceramint.2022.03.093.

45 F. Luo, D. Q. Liu, T. S. Cao and H. F. Cheng, *et al.*, Study on broadband microwave absorbing performance of gradient porous structure, *Adv. Composites Hybrid Mater.*, 2021, **4**(3), 591–601, DOI: 10.1007/s42114-021-00275-4.

46 M. Rebber, M. Trommler, I. Lokteva and S. Ehteram, *et al.*, Additive-Free, Gelled Nanoinks as a 3D Printing Toolbox for Hierarchically Structured Bulk Aerogels, *Adv. Funct. Mater.*, 2022, **32**(19), 2112914, DOI: 10.1002/adfm.202112914.

47 Y. Liu, Y. Li, K. Zhao and M. G. B. Drew, *et al.*, Microwave absorption properties of Ag/$NiFe_{2-x}Ce_xO_4$ characterized by an alternative procedure rather than the main stream method using ''reflection loss'', *Mater. Chem. Phys.*, 2020, **243**, 122615, DOI: 10.1016/j.matchemphys.2019.122615.

48 S. S. S. Afghahi, A. Shokuhfar, B. Saberi and A. Javidan, Iron-cobalt-graphite core–shell nanoparticles as efficient electromagnetic wave absorbers at X-band frequency range, *Micro Nano Lett.*, 2014, **9**(6), 412–416, DOI: 10.1049/mnl.2013.0723.

49 M. Song, C. Wang, C. Zhu and T. C. You, *et al.*, An effective fabrication and highly tunable microwave absorption of nitrogen-doped graphene, *Diamond Relat. Mater.*, 2022, **129**, 109348, DOI: 10.1016/j.diamond.2022.109348.

50 J. Zhou, D. Liu, Y. Xiong and Y. Akinay, A novel approach to prepare polyaniline/Polypyrrole@Cu-BTC/NH2-MIL 101(Fe) MOFs for electromagnetic wave absorption, *Ceram. Int.*, 2020, **46**(12), 19758–19766, DOI: 10.1016/j.ceramint.2020.05.006.

51 A. M. Gama and M. C. Rezende, Complex Permeability and Permittivity Variation of Radar Absorbing Materials Based on MnZn Ferrite in Microwave Frequencies, *Mater. Res.-Ibero-American J. Mater.*, 2013, **16**(5), 997–1001, DOI: 10.1590/s1516-14392013005000077.

52 S. Zhang, Y. H. Zhai and Y. Zhang, Microwave-absorbing performance and mechanical properties of poly(vinyl chloride)/acrylonitrile-butadiene rubber thermoplastic elastomers filled with multiwalled carbon nanotubes and silicon carbide, *J. Appl. Polym. Sci.*, 2013, **130**(1), 345–351, DOI: 10.1002/app.39063.

53 L. Huang, M. Wang, L. C. Cheng and S. K. Pan, *et al.*, Fast and efficient synthesis of a new adjustable perovskite-structured ferrite $La_{1-x}Ca_xFeO_3$ microwave absorbent, *J. Alloys Compd.*, 2022, **892**, 162167, DOI: 10.1016/j.jallcom.2021.162167.

54 Z. Xing, C. J. Shen, C. Z. Yin and H. J. Ye, *et al.*, Low temperature synthesis and dielectric characterisation of $La_2Mo_2O_9$ ceramic at RF and microwave frequencies, *Adv. Appl. Ceram.*, 2020, **119**(7), 387–392, DOI: 10.1080/17436753.2020.1774220.

55 H. Y. Wei, Z. P. Zhang, G. Hussain and L. S. Zhou, *et al.*, Techniques to enhance magnetic permeability in microwave absorbing materials, *Appl. Mater. Today*, 2020, **19**, 100596, DOI: 10.1016/j.apmt.2020.100596.

56 L. Liu, N. He, T. Wu and P. B. Hu, *et al.*, Co/C/Fe/C hierarchical flowers with strawberry-like surface as surface plasmon for enhanced permittivity, permeability, and microwave absorption properties, *Chem. Eng. J.*, 2019, **355**, 103–108, DOI: 10.1016/j.cej.2018.08.131.

57 L. X. Wang, Y. K. Guan, X. Qiu and H. L. Zhu, *et al.*, Efficient ferrite/Co/porous carbon microwave absorbing material based on ferrite@metal-organic framework, *Chem. Eng. J.*, 2017, **326**, 945–955, DOI: 10.1016/j.cej.2017.06.006.

58 A. Kumar and S. Asthana, Investigations on structural, dielectric, and impedance properties of ecofriendly Ho^{3+}/Nb^{5+} co-substituted Na-0.5 $Bi_{0.5}TiO_3$, *J. Alloys Compd.*, 2022, **927**, 166958, DOI: 10.1016/j.jallcom.2022.166958.

59 K. S. Cole and R. H. Cole, Dispersion and Absorption in Dielectrics I. Alternating Current Characteristics, *J. Chem. Phys.*, 1941, **9**(4), 341.

60 H. Zhang, Q. J. Ding, G. Zhao and J. F. Song, Synthesis of $NiCo_2O_4$/CF composites with heterogeneous interfaces as excellent microwave absorbers, *Mater. Today Commun.*, 2023, **37**, 106919, DOI: 10.1016/j.mtcomm.2023.106919.

61 R. Peymanfar, M. Ahmadi and S. Javanshir, Tailoring GO/$BaFe_{12}O_{19}La_{0.5}Sr_{0.5}MnO_3$ ternary nanocomposite and investigation of its microwave characteristics, *Mater. Res. Express*, 2019, **6**(8), 085063.

62 X. Zhang, X. C. Zhang, D. T. Wang and H. R. Yuan, *et al.*, Three dimensional graphene-supported nitrogen-doped carbon nanotube architectures for attenuation of electromagnetic energy, *J. Mater. Chem. C*, 2019, **7**(38), 11868–11878, DOI: 10.1039/c9tc04191e.

63 Y. H. Hou, H. L. Yuan, H. Chen and J. H. Shen, *et al.*, Controlled fabrication and microwave absorbing mechanism of hollow Fe_3O_4@C microspheres, *Sci. China: Chem.*, 2017, **60**(6), 740–747, DOI: 10.1007/s11426-016-9001-5.

64 H. P. Lv, C. Wu, F. X. Qin and H. X. Peng, *et al.*, Extra-wide bandwidth via complementary exchange resonance and dielectric polarization of sandwiched FeNi@SnO_2 nanosheets for electromagnetic wave absorption, *J. Mater. Sci. Technol.*, 2021, **90**, 1–8, DOI: 10.1016/j.jmst.2020.12.083.

65 J. Y. Yusuf, H. Soleimani, N. Yahya and Y. K. Sanusi, *et al.*, Recent advances and prospect of cobalt based microwave absorbing materials, *Ceram. Int.*, 2020, **46**(17), 26466–26485, DOI: 10.1016/j.ceramint.2020.07.244.

66 Y. Cheng, H. Q. Zhao, Y. Zhao and J. M. Cao, *et al.*, Structure-switchable mesoporous carbon hollow sphere framework toward sensitive microwave response, *Carbon*, 2020, **161**, 870–879, DOI: 10.1016/j.carbon.2020.02.011.

67 G. L. Song, L. X. Gai, K. K. Yang and X. T. Wang, *et al.*, A versatile N-doped honeycomb-like carbonaceous aerogels loaded with bimetallic sulfide and oxide for superior electromagnetic wave absorption and supercapacitor applications, *Carbon*, 2021, **181**, 335–347, DOI: 10.1016/j.carbon.2021.05.044.

68 H. H. Wang, Q. D. An, Z. Y. Xiao and Y. Tong, *et al.*, Marine polysaccharide-based electromagnetic absorbing/shielding materials: design principles, structure, and properties, *J. Mater. Chem. A*, 2022, **10**(33), 17023–17052, DOI: 10.1039/d2ta03529d.

69 Y. C. Wang, L. H. Yao, Q. Zheng and M. S. Cao, Graphene-wrapped multiloculated nickel ferrite: a highly efficient electromagnetic attenuation material for microwave absorbing and green shielding, *Nano Res.*, 2022, **15**(7), 6751–6760, DOI: 10.1007/s12274-022-4428-x.